Patterning Complex Line Motifs in Thin Films Using Immersion Controlled Reaction-Diffusion

Christiaan T. van Campenhout, Hinco Schoenmaker, Martin van Hecke, Willem L. Noorduin**

C.T. van Campenhout[1], H. Schoenmaker[1], M. van Hecke[1,2], W. L. Noorduin[1,3]
[1]AMOLF, Science Park 104, 1098XG Amsterdam, The Netherlands
[2]Leiden Institute of Physics, Leiden University, Niels Bohrweg 2, 2333 CA Leiden, The Netherlands
[3]Van 't Hoff Institute for Molecular Sciences, University of Amsterdam, Science Park 904, Amsterdam 1090 GD, The Netherlands
Email Address: mvhecke@gmail.com, noorduin@amolf.nl

Keywords: *Reaction-Diffusion, Pattern Formation, Liesegang Patterning, Hierarchical Materials, Moiré Patterns*

The discovery of self-organization principles that enable scalable routes towards complex functional materials has proven to be a persistent challenge. Here reaction-diffusion driven, immersion controlled patterning (R-DIP) is introduced, a self-organization strategy using immersion controlled reaction-diffusion for targeted line patterning in thin films. By modulating immersion speeds, the movement of a reaction-diffusion front over gel films is controlled, which induces precipitation of highly uniform lines at the reaction front. A balance between the immersion speed and diffusion provides both hands-on tunability of the line spacing ($d = 10 - 300$ μm) as well as error-correction against defects. This immersion-driven patterning strategy is widely applicable, which is demonstrated by producing line patterns of silver/silver oxide nanoparticles, silver chromate, silver dichromate, and lead carbonate. Through combinatorial stacking of different line patterns, hybrid materials with multi-dimensional patterns such as square-, diamond-, rectangle- and triangle-shaped motifs are fabricated. The functionality potential and scalability is demonstrated by producing both wafer-scale diffraction gratings with user-defined features as well as an opto-mechanical sensor based on Moiré patterning.

1 Introduction

Nature's extraordinary diversity of complex patterns holds fascination to lay people and scientists alike, and provides an endless source of inspiration for developing new materials with advanced functionalities [1–9]. Specifically, thins films with complex motifs are of great interest as these can be integral to the next generation of optical, electronic, and mechanical devices [10–12]. However, manufacturing of such motifs has remained challenging, with costly lithography techniques being the leading method to produce nanoscale complexity [13–16]. From this perspective, bio inspired self-organization can be an attractive starting point, as the inherent autonomous nature of such processes holds the potential to offer simple and scalable production of uniform complex patterns with user-defined control and automatic error correction for tolerance against defects [17–20]. Already, many self-organization strategies have been developed, such as evaporative assembly and dip-pen nano-lithography [21–26], but whilst such processes are able to produce highly uniform patterns, delicate and extremely precise setups are often required and scalability can be difficult or practically impossible.

Alternatively, self-organization of patterns is possible via reaction-diffusion processes, in which the interplay between reaction kinetics and diffusion can induce complex patterns spontaneously [27–29]. Since these processes rely on chemical feedback loops, there is the potential to achieve inherent error-correction towards robustness for large scale production of uniform patterns [8]. Moreover, reaction-diffusion processes such as Liesegang pattern formation induce rhythmic precipitation of line or band patterns of many different chemical compositions, and combinations with top-down fabrication techniques such as wet-stamping can yield more complex patterns [30–35]. Unfortunately, because of the diffusive nature of these processes, lines or bands form at increasing spacing, resulting in non-uniform patterning over larger scales, hence limiting scalability [36]. To overcome such drawbacks, we recently have shown highly uniform banding patterns in bulk gels by employing a mechano-chemical feedback loop that transports reagents non-diffusively through opening channels [37]. However, because mechanical opening of a transport channel is integral to the approach, this strategy only works for three-dimensional materials, highlighting that entirely new principles need to be developed to achieve uniform large-scale patterning of complex motifs in thin films.

This article has been accepted for publication and undergone full peer review but has not been through the copyediting, typesetting, pagination and proofreading process, which may lead to differences between this version and the Version of Record. Please cite this article as doi: 10.1002/adma.202305191

Here we introduce reaction-diffusion driven immersion-controlled patterning (R-DIP), a method for creating complex line motifs in thin films on wafer scale with user-defined tunability (**Figure 1A**). First, R-DIP is used to pattern uniform lines with user-defined spacing in thin gel films. Second, multiple thin films with different line patterns and chemical compositions are superimposed in combinatorial stacks to realize complex composites and hybrid motifs. Using this strategy, we demonstrate that a large diversity of complex, yet well-defined motifs such as squares, diamonds, rectangles and triangles can be realized, and exploit this control to develop tunable diffraction gratings and opto-mechanical sensors.

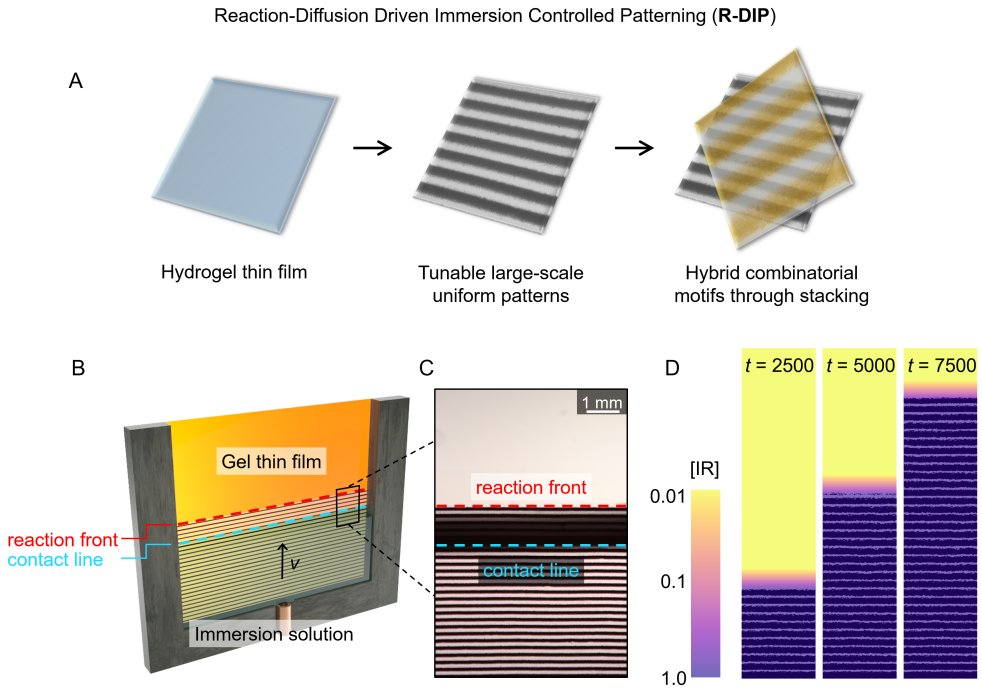

Figure 1: (A) Overview of the R-DIP process: first a hydrogel thin film is cast, in which an immersion controlled reaction-diffusion process generates large-scale uniform stripe patterns. Multiple of these user-defined patterns can be stacked to produce a large diversity of higher-order composites and hybrid motifs. (B) Concept image depicting the experimental setup: a gel film containing gel reagent is placed in an empty container, into which immersion reagent (IR) is pumped with a syringe pump, steadily immersing the thin film. Preceding the liquid-gel contact line (depicted in blue) at the reaction front (depicted in red) the reaction between the immersion and gel reagent produces a line pattern of precipitate perpendicular to the immersion direction. At constant immersion speed a balance between the immersion speed v and upward diffusion is reached, resulting in highly uniform line distances (d). (C) A close-up during the patterning process process reveals the formation of a highly uniform line pattern of silver dichromate precipitate at the reaction front (see Movie S1). (D) Numerical modeling accurately reproduces the experimental pattern and provides mechanistic insights. During the process, the concentration gradient of silver ions at the liquid-gel interface remains constant and therefore patterning is uniform (see Experimental Section for details on the numerical model).

The key idea behind R-DIP is that a thin gel film, in which one reagent (the gel reagent) is dissolved, is steadily immersed into a solution of a second reagent (the immersion reagent), which react upon contact at the reaction front to induce rhythmic precipitation of an insoluble reaction product (Figure 1B). This reaction product forms highly uniform equidistant line patterns because of a balance between the immersion speed (v) and upwards diffusion of the immersion reagent into the gel film. Consequently, a constant concentration gradient of immersion reagent is maintained at the reaction front, which induces uniform pattern formation. Additionally, because the process relies on chemical feedback loops, it possesses inherent error-correction, enabling large scale production of user-defined line motifs.

2 Results and Discussion

Figure 1B shows the general method of inducing pattern formation with immersion-controlled reaction-diffusion. We demonstrate the proof of principle for the well-studied periodic precipitation of silver dichromate ($Ag_2Cr_2O_7$) using silver nitrate as immersion reagent and potassium dichromate as gel reagent following: $2Ag^+(aq) + Cr_2O_7{}^{2-}(aq) \rightarrow Ag_2Cr_2O_7(s)$ [38].

Typically, we cast thin hydrogel films consisting of gelatin (10 wt%), agarose (0.5 wt%), potassium dichromate ($K_2Cr_2O_7$, 0.2 wt%), acetic acid (0.9 %v/v) and the surfactant 3-[hydroxy(polyethyleneoxy) propyl] heptamethyltrisiloxane (HPEO-HMTS, 0.15 %v/v) onto glass slides (75x50 mm, see the Experimental Section for details). These components have the following functions: gelatin promotes pattern formation [39]; agarose offers additional mechanical gel stability; potassium dichromate acts as the gel reagent; acetic acid ensures that the dichromate-chromate equilibrium is shifted towards the desired dichromate anion [40]; and the surfactant prevents pinning of the immersion solution on the gel surface. Note that gel films are thin (<0.6 mm) to ensure that patterning is consistent throughout the depth of the film. To start the process, the gel film is mounted vertically in an empty container. Then, patterning is induced by filling the container at user-defined speeds with the immersion reagent silver nitrate ($AgNO_3$, 0.4 M in water). The filling results in a moving liquid-gel contact line with speed v and in precipitation of separate $Ag_2Cr_2O_7$ particles that arrange in lines perpendicular to the immersion direction. We monitor this pattern formation over long distances by tracking the moving contact line with a custom motorized horizontal microscope (see Figure S1 for details). We observe the formation of a line pattern with highly uniform spacing ($d = 200 \pm 6$ µm) throughout the entirety of the thin film (Figure 1C, Movie S1).

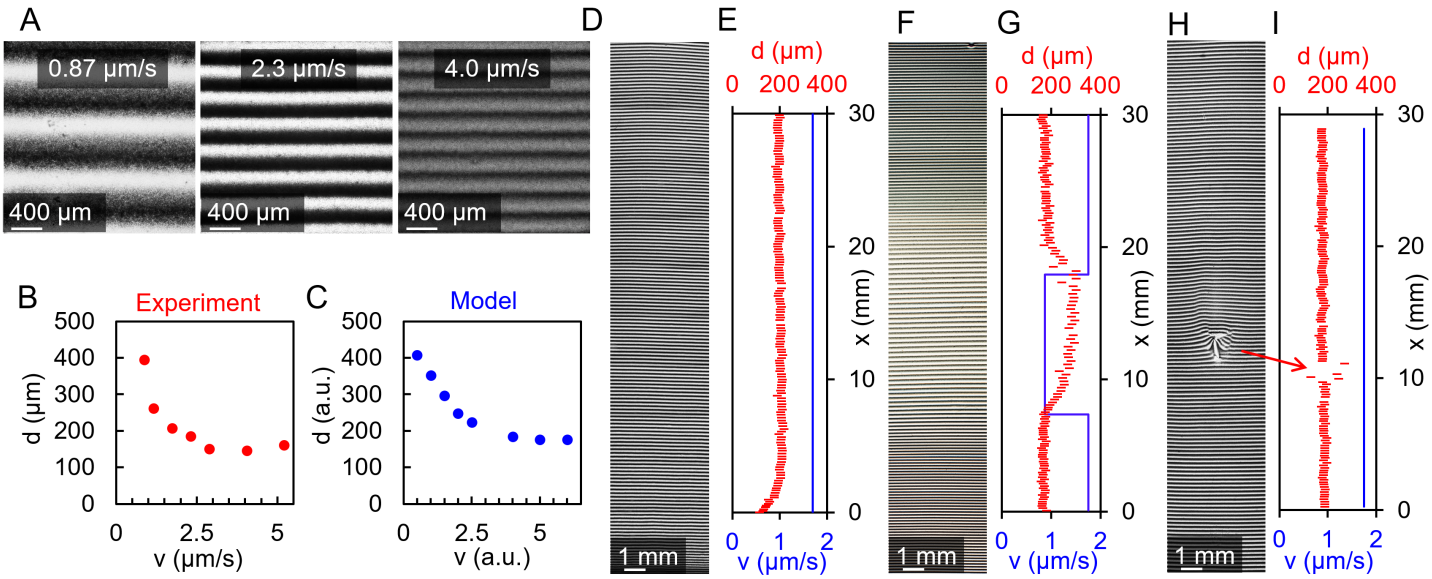

Figure 2: Patterning tunability (A) Experimentally obtained patterns for a range of immersion speeds v (B, C) Plotting the line distance d versus the immersion speed v for both the model and the experiments shows a trend of decreasing d for increasing v. (D, E) Large scale pattern obtained at constant v with highly uniform line spacing ($d = 200 \pm 6$ µm). (F, G) Dynamic tunability in a silver dichromate pattern by changing v during pattern formation showing that modulating v directly translates to a change in line distance d. (H, I) Patterning is self-correcting and recovers to the original line pattern swiftly after encountering a defect in the thin film. Note that the figures D, F and H are stacks composed of multiple images.

To explain this uniform pattern formation, we numerically model the 2D reaction-diffusion process. In this model, we replicate gel immersion by calculating the location of the contact line at every time-step and setting the concentration of immersion reagent equal to the starting concentration up to this location. All reactants diffuse following a forward-in-time-central-in-space scheme, and the reaction of the gel and immersion reagent is computed using first- and second-order reaction kinetics (see the Experimental Section for further details). This model accurately reproduces the observed uniformity and immersion speed

dependent line spacing. Monitoring concentration gradients in the model reveals the formation of a steady-state which balances the upwards diffusion of immersion reagent into the gel and the immersion speed v (Figure 1D). Because of this steady-state, the concentration gradient of immersion reagent at the reaction front remains constant, thereby inducing uniform pattern formation.

The intricate interplay between diffusion of silver ions and immersion speed suggests that by modulating v we can tune the line distance d. Indeed, we find that increasing v results in decreasing line widths (**Figure 2A**), both in experiments (Figure 2B) and in our model (Figure 2C). This allows us to precisely tune the line pattern by controlling the immersion speed. At constant v, patterning is uniform over long distances (Figure 2D, E). Because pattern formation is directly dependent on the user-defined speed of the contact line, we can dynamically tune patterning within a thin film (Figure 2F, G). We demonstrate this dynamic tunability by modulating v from fast to slow ($v = 1.75 \rightarrow 0.87$ µm/s), which increases the line distance ($d = 172 \rightarrow 290$ µm). After going back to the initial immersion speed ($v = 1.75$ µm/s), the patterning restores to the initial spacing ($d = 172$ µm). Thus, v is directly tied to a specific line distance d and can be tuned during the process, enabling rational and precise steering of the self-organization process.

The uniformity of the pattern formation across large distances suggests that R-DIP has an inherent error-correction mechanism. To study this error-correction mechanism, we deliberately damage the gel film and subsequently follow how pattern formation is influenced by this defect (Figure 2H, I). As soon as the reaction front reaches the defect, the reaction front and pattern become disturbed. However, already after fewer than 10 lines the reaction front is smoothened out by diffusion and subsequently deposited lines are straight again, demonstrating that R-DIP indeed offers error-correction for sustaining uniform micro-scale ordering over decimeter distances. The steady-state conditions at the reaction front thus offer both swift responsiveness to changes in the immersion speed and error-correction for defect tolerance.

Because R-DIP produces large-scale gel films containing uniform patterns of precipitate, where the gel matrix provides mechanical stability and thus transferability to the patterned thin films, we can produce higher-order complexity by stacking multiple user-defined line patterns. Here we provide some exemplary cases to illustrate this combinatorial approach (**Figure 3**). For example, by aligning and stacking two identical line patterns at 90°or 42°, we create highly regular square- or diamond motifs (Figure 3A, B). Because our strategy yields tunable line patterns, the line spacing of each layer can be selected independently, for instance allowing the formation of rectangle motifs by stacking two non-identical line patterns (Figure 3C).

Moreover, R-DIP can be readily applied to many other reaction-diffusion processes, enabling patterning of different chemical compositions and the manufacturing of multi-material hybrid motifs. To demonstrate this versatility we produce patterns of three additional materials: lead carbonate, silver chromate, and silver/silver oxide nanoparticles. For lead carbonate patterns, we modify a Liesegang patterning process developed by Isemura in 1936 [41], using lead acetate as immersion reagent and sodium carbonate as gel reagent to produce diamond patterns of lead carbonate (Figure 3D, see the Experimental Section for more details). Since each thin film pattern is formed independently, we can produce hybrid motifs by superimposing thin films with patterns of different materials, which we illustrate by producing a rectangular pattern of lead carbonate on silver dichromate (Figure 3E).

To display the application potential of R-DIP, we assemble tunable optical diffraction gratings with microscopic line patterns of both silver chromate and of silver nanoparticles. First, we react silver nitrate ($AgNO_3$) as immersion reagent with potassium chromate (K_2CrO_4) as gel reagent to precipitate microscopic lines of silver chromate ($d = 31$ µm). Then, by stacking these microscopic line patterns, we manufacture square and diamond motifs (Figure 3F, G), which upon irradiation with a green laser ($\lambda = 532$ nm) show distinct diffraction patterns that are in good agreement with the microscopic structure (diffraction: $d = 32$ µm, directly observed: $d = 31$ µm). To produce microscopic line patterns of silver/silver oxide nanoparticles, we adapt a previously developed precipitation system, where patterning is induced by the reduction of silver nitrate in a gelatin film containing a small amount of ammonia [42]. Stacking three of these patterns at 60°angles yields a triangular diffraction grating (Figure 3H), where again the spacing is in good agreement with the microscopic structure (diffraction: $d = 15.5$ µm, directly observed: $d = 15$ µm), hence illustrating that such self-organized patterns can serve as diffraction gratings with user-defined

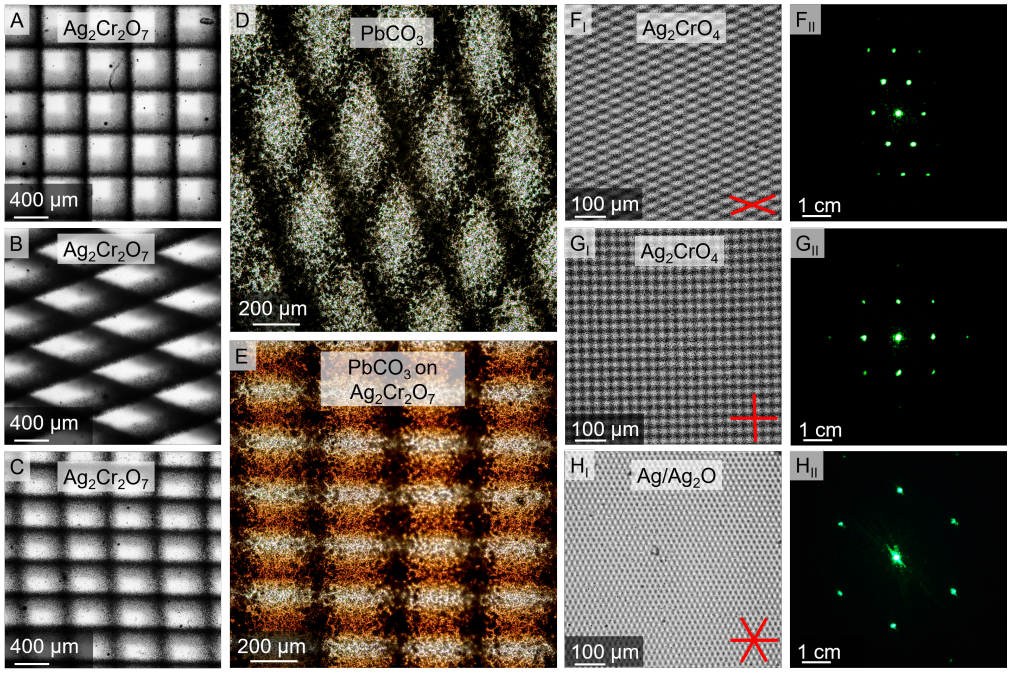

Figure 3: Aligning and stacking thin films generates higher-order patterning. All images are taken with a light microscope in transmission mode. (A, B) Stacking of identical silver dichromate patterns ($d_1 = d_2 = 285$ µm) at 90° and 42° angles yields square and diamond motifs respectively. (C) Stacking two patterns with non-identical line spacing ($d_1 = 206$ µm, $d_2 = 300$ µm) results in a rectangular motif. (D) Diamond motif produced by superimposing two identical line patterns of lead carbonate. (E) Rectangular hybrid motif produced by superimposing a line pattern of silver dichromate (orange-brown) with a line pattern of lead carbonate (black). (F, G) Diamond and square motifs produced by stacking identical line patterns $d = 31$ µm of silver chromate. Irradiating these microscopic patterns with a green laser ($\lambda = 532$ nm) produces a diffraction pattern that is in good agreement with the microscopic spacing ($d = \frac{m\lambda}{2sin(\theta)}$, diffraction: $d = 32$ µm, directly observed: $d = 31$ µm). (H) Triangular pattern produced by stacking three identical microscopic line patterns $d = 15$ µm of silver/silver oxide nanoparticles, and the diffraction pattern obtained upon irradiation of this pattern with a green laser ($\lambda = 532$ nm).

tunability.

We demonstrate the scalability potential of R-DIP by taking advantage of the simplicity, inherent autonomous nature, and error-correction of our pattern formation process to produce a wafer-scale diffraction grating. For this demonstration, we precipitate silver/ silver oxide nanoparticles in a gelatin film to demonstrate large scale patterning using only non-toxic materials. We achieve this by first casting a gelatin film containing a small amount of ammonia onto an A4-sized flexible acetate support sheet (21x29.7 cm), and subsequently inducing pattern formation by slowly immersing the film into a solution of silver nitrate (0.4M) (**Figure 4A**). After drying, this gel film is easily removed from the acetate support sheet to obtain a wafer-scale flexible thin-film (Figure 4B) containing a highly uniform pattern consisting of more than 20000 microscopic lines of silver/silver oxide nanoparticles that each have a well-defined and uniform spacing (Figure 4C), and which act as a diffraction grating throughout the entire film (Movie S3).

To further explore the functionality potential of R-DIP and specifically demonstrate the large-scale uniformity of our approach, we manufacture an opto-mechanical sensor based on Moiré patterning. When two identical line-patterns are separated by a flexible spacer and aligned parallel, a compression sensor is made. Because deformation of such a sensor induces a misalignment of the two line patterns, higher-order Moiré patterns emerge, with a wavelength dependent on the amount of compression. In this example, we superimpose two identical line patterns of silver dichromate ($d = 200$µm), which upon compression reveal macroscopic Moiré patterns (Figure 4D, Movie S4). The Moiré patterning wavelength (λ) is directly correlated to the amount of compression (c) with $c \propto \lambda^{-1}$ (Figure 4E), and can thus be used as a readout for compression, demonstrating the functionality potential of uniform patterning with microscopic precision in flexible films.

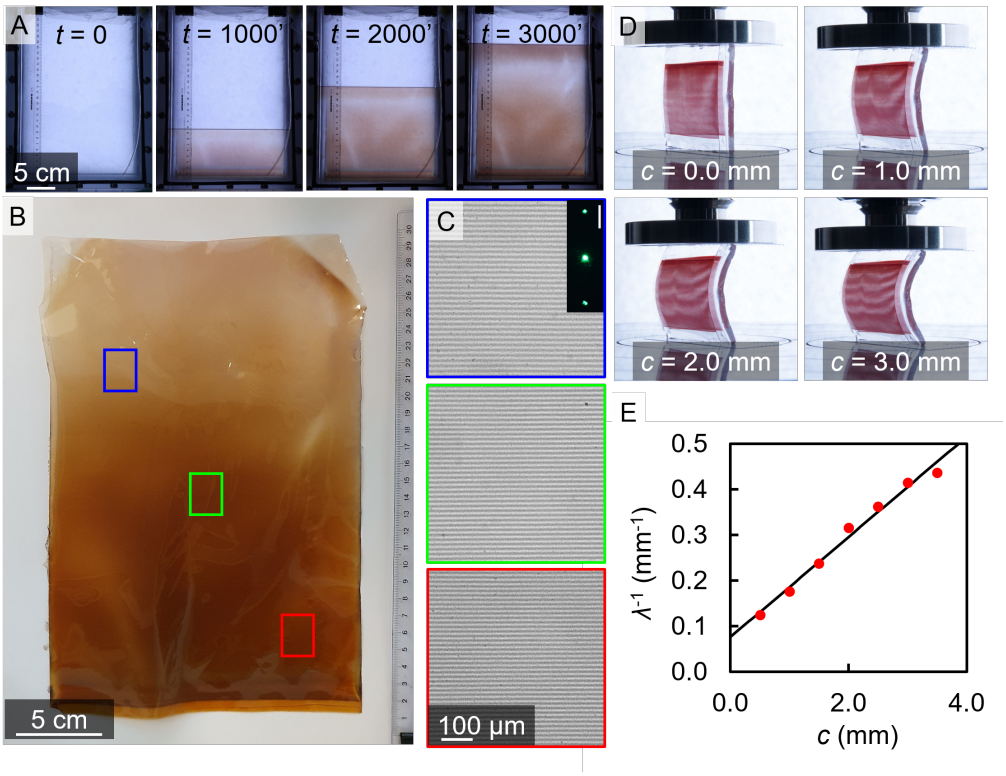

Figure 4: Scalability and applicability of R-DIP. (A) Snapshots at various times during the wafer-scale patterning of silver/silver oxide micropatterns (see Movie S2). (B) Macroscopic image of the dried A4-sized thin-film after patterning. Note that the precipitated material intensifies during light exposure, which causes a slight color gradient throughout the film. (C) Post-patterning analysis of the wafer-scale pattern, revealing a highly uniform microscopic pattern throughout the entirety of the film. Inset shows the diffraction pattern obtained by irradiating the dried film with a 532 nm laser (see Movie S3, scale-bar = 1 cm). (D) Optomechanical sensor composed of two parallel aligned identical stripe patterns that are separated by a spacer, such that compression results in the emergence of Moiré patterns (see Movie S4). (E) Plot showing the amount of compression (c) versus the inverse of the observed Moiré pattern wavelength (λ^{-1}), with in black a linear fit to this relationship

3 Conclusion

Here we introduce reaction-diffusion driven immersion-controlled patterning (R-DIP) as method for creating complex user-defined line motifs in thin films. The power of this patterning strategy is that we exploit autonomous self-organization to create tunable equidistantly spaced microscale lines at wafer-scale that can combinatorially be superimposed into complex hybrid motifs. To demonstrate the functionality potential, we leverage our control over patterning and create tunable diffraction gratings and a sensitive mechanical sensor. An intriguing next step will be downscaling of the pattern spacing to sub-micrometer dimensions, to achieve for instance functionalities such as structural color or optical polarizers. The challenge in downscaling patterning is that the minimal line spacing is mainly controlled by the rate of nucleation [43], which may be optimized by incorporating nucleation promoters in the gel matrix or by inducing pattern formation at different temperatures.

To demonstrate the proof-of-principle, we apply R-DIP for four different precipitation systems, but we anticipate that extension of this method is straightforwardly possible to many other chemical compositions. For this, the main requirement is that the combination of inner and out reagent results in abrupt self-limiting precipitation of a product. For many nanoparticle or metal-organic-framework syntheses this requirement is met, and recent work shows that combining such syntheses with reaction-diffusion provides control over morphology and size [44,45]. Combining these methods with R-DIP could therefore introduce an additional level of control and provide uniformity to the sizes and morphologies obtained. As such, we foresee that R-DIP can open routes to a large library of material compositions with interesting chemical, electronic or optical properties that can find applications in for instance optical gratings for spectrometers

[46], capacitors for electronic devices [47] or electromagnetic shielding [48]. Moreover, we foresee that R-DIP can be extended to entirely different systems based on for instance polymerization or phase-separation, thus opening many directions for self-organizing a large diversity of chemical compositions. Additionally, the simplicity, autonomous nature and inherent error-correction of R-DIP offers opportunities for robust manufacturing and practical scale-up. Specifically, we recognize that the immersion step and flexibility of the films can be exploited to translated R-DIP into a roll-to-roll process, in which a film is pulled through a solution with immersion reagent to achieve continuous pattern production. Intriguingly, faster immersion results in smaller patterns, such that, almost counter intuitively, faster production yields smaller patterns. Overall, R-DIP offers a versatile and scalable approach for creating complex user-defined line motifs in thin films, enabling a wide range of applications in materials science and manufacturing.

4 Experimental Section

In this section we first state all patterning recipes used, after which we describe the gel casting procedure and the patterning process, and lastly the numerical model is introduced. All chemicals were used without additional purification. Gelatin was purchased from Sigma-Aldrich and was type A from porcine skin (roughly 300 g Bloom). Agarose was purchased from Sigma-Aldrich and was of type I, with low EEO. 3-[hydroxy(polyethyleneoxy)propyl] heptamethyltrisiloxane (CAS: 67674-67-3) was purchased from Gelest.

Wetting Agent:
To mitigate detrimental effects of uneven wetting, we modify the gel by adding a wetting agent. Specifically, we add 3-[hydroxy(polyethyleneoxy)propyl] heptamethyltrisiloxane (HPEO-HMTS), which ensures complete wetting of the gelatin surface, completely negating any surface effects, without affecting pattern formation inside of the gel.

$Ag_2Cr_2O_7$ patterning gel recipe:
Gelatin (2.0 g), potassium dichromate (40 mg), HPEO-HMTS (30 µL) and glacial acetic acid (180 µL) are added to DI water (13 mL). This mixture is heated to 65 °C to dissolve gelatin. Simultaneously, a solution of agarose (0.1 g) in water (5 mL) is prepared by microwave heating. These two solutions are combined at 65 °C to yield a liquid gel solution, which sets after cooling to room temperature. Patterning is then induced with an immersion reagent solution of silver nitrate (0.4 M) and acetic acid (0.9 v/v %).

Ag_2CrO_4 patterning gel recipe:
Gelatin (2.0 g), potassium chromate (40 mg), HPEO-HMTS (30 µL) and ammonia (25% in water, 240 µL) are added to DI water (13 mL). This mixture is heated to 65 °C to dissolve gelatin. Simultaneously, a solution of agarose (0.1 g) in water (5 mL) is prepared by microwave heating. These two solutions are combined at 65 °C to yield a liquid gel solution, which sets after cooling to room temperature. Patterning is then induced with an immersion reagent solution of silver nitrate (0.4 M in water).

$PbCO_3$ patterning gel recipe:
Gelatin (0.5 g) and potassium carbonate (166 mg) are added to DI water (13 mL). This mixture is heated to 65 °C to dissolve gelatin. Simultaneously, a solution of agarose (0.1 g) in water (5 mL) is prepared by microwave heating. These two solutions are combined at 65 °C to yield a liquid gel solution, which sets after cooling to room temperature. Patterning is then induced with an immersion reagent solution of lead acetate (1.0 M in water).

Gel Casting Procedure:
Gels are typically cast onto large microscopy glass slides (75x50 mm). First, we preheat these slides to > 65 °C to ensure that gels do not instantly solidify on the glass surface. Then we place a glass slide in a custom holder with edges 0.5 mm taller than the thickness of the glass slide. Roughly 2 mL of hot gel solution is

then added onto the glass slide and spread out evenly with a polyoxymethylene (non-stick) block, resulting in a 0.5 mm layer of gel covering one side of the glass slide. After cooling to room temperature, the gel sheets have solidified and are ready for use.

Inducing pattern formation:
After the gel films have solidified, they are mounted vertically in an empty chamber. Using a syringe pump, the immersion reagent solution is then added to the bottom of this chamber through PTFE tubing, filling the chamber. Note that the gel film is stationary, but by introducing immersion reagent we are effectively immersing the film (See Figure 1A for a schematic of this setup and supporting Figure S1 for a detailed explanation on the pattern formation setup).

Wafer-scale patterning of silver nanoparticles:
First, gelatin (4.0 g), HPEO-HMTS (60 µL) and ammonia (25% in water, 180 µL) are added to DI water (36 mL)). This mixture is heated to 60°C to dissolve the gelatin. In a special holder, an A4 sized acetate support film is mounted, with a 0.5 mm frame on top. The hot gelatin solution is then poured onto the acetate film and spread evenly with a plastic fondant smoother. This yields a roughly 0.5 mm thick A4 gel sheet on an acetate support. Similarly to previous experiments, albeit scaled up to accommodate the large-scale sheet, the sheet is mounted vertically in an empty chamber, into which silver nitrate (0.4M in water) is slowly pump by a peristaltic pump.

Numerical model:
The model is partially based on previous work [37], with two significant changes: the model shown here is 2D instead of 1D and incorporates a moving contact line. The reaction-diffusion system modeled here is the periodic precipitation of silver dichromate in a gelatin hydrogel as a result of silver nitrate diffusing into the gel matrix and reacting with potassium dichromate to produce an insoluble salt (Equation 1):

$$2\mathrm{Ag}^{+}(aq) + \mathrm{Cr_2O_7}^{2-}(aq) \rightarrow \mathrm{Ag_2Cr_2O_7}(s) \tag{1}$$

In this pre-nucleation model, this reaction is split into three steps: 1. sol formation, 2. nucleation and 3. growth.

1. First a sol of $\mathrm{Ag_2Cr_2O_7}$ is formed (Equation 2):

$$2\mathrm{Ag}^{+}(aq) + \mathrm{Cr_2O_7}^{2-}(aq) \underset{k_1}{\longrightarrow} \mathrm{Ag_2Cr_2O_7}(aq). \tag{2}$$

2. This sol only nucleates after a specified nucleation threshold c^* is exceeded (Equation 3):

$$\mathrm{Ag_2Cr_2O_7}(aq) \underset{k2}{\longrightarrow} \mathrm{Ag_2Cr_2O_7}(s). \tag{3}$$

3. Growth onto these nuclei is auto-catalytic and extremely rapid (Equation 4):

$$\mathrm{Ag_2Cr_2O_7}(aq) + \mathrm{Ag_2Cr_2O_7}(s) \underset{k3}{\longrightarrow} 2\mathrm{Ag_2Cr_2O_7}(s). \tag{4}$$

These reactions form the basis for a set of reaction-diffusion equations, where we assume a two dimensional geometry (Equations 5 - 8):

$$\frac{\partial[\mathrm{Ag}^{+}]}{\partial t} = D\left(\frac{\partial^2[\mathrm{Ag}^{+}]}{\partial x^2} + \frac{\partial^2[\mathrm{Ag}^{+}]}{\partial y^2}\right) - 2k_1[\mathrm{Ag}^{+}][\mathrm{Cr_2O_7}^{2-}], \tag{5}$$

$$\frac{\partial[\mathrm{Cr_2O_7}^{2-}]}{\partial t} = D\left(\frac{\partial^2[\mathrm{Cr_2O_7}^{2-}]}{\partial x^2} + \frac{\partial^2[\mathrm{Cr_2O_7}^{2-}]}{\partial y^2}\right) - 2k_1[\mathrm{Ag}^{+}][\mathrm{Cr_2O_7}^{2-}], \tag{6}$$

$$\frac{\partial[\mathrm{Ag_2Cr_2O_7}]_{\mathrm{aq}}}{\partial t} = D(\frac{\partial^2[\mathrm{Ag_2Cr_2O_7}]_{aq}}{\partial x^2} + \frac{\partial^2[\mathrm{Ag_2Cr_2O_7}]_{aq}}{\partial y^2}) + 2k_1[\mathrm{Ag^+}][\mathrm{Cr_2O_7}^{2-}] - k_2[\mathrm{Ag_2Cr_2O_7}]_{aq}\theta([\mathrm{Ag_2Cr_2O_7}]_{aq} - c^*) - k_3[\mathrm{Ag_2Cr_2O_7}]_{aq}[\mathrm{Ag_2Cr_2O_7}]_s, \quad (7)$$

$$\frac{\partial[\mathrm{Ag_2Cr_2O_7}]_s}{\partial t} = k_2[\mathrm{Ag_2Cr_2O_7}]_{aq}\theta([\mathrm{Ag_2Cr_2O_7}]_{aq} - c^*) + k_3[\mathrm{Ag_2Cr_2O_7}]_{aq}[\mathrm{Ag_2Cr_2O_7}]_s. \quad (8)$$

These equations describe the classical Liesegang system, where bands or stripes form progressively further and further apart. To incorporate immersion speeds, we introduce a time-dependent immersion reagent interface, which moves at a constant speed (Equation 9):

$$y_{int} = v \times t \quad (9)$$

Subsequently, for all immersed points we set the concentration of immersion reagent ($[Ag]_{y<y_{int}}$) as equal to the starting concentration ($[Ag]_0$). To compensate for dilution effects we take the total volumes of outer and gel reagent (V_{out} and V_{in} respectively) into account, as well as the portion of the chamber that has been filled (β). (Equation 10):

$$[Ag]_{x<x_{int}} = [Ag]_0 \times \frac{V_{out}}{V_{out} + \beta V_{in}} \quad with\ \beta = \frac{y_{int}}{l_{system}}. \quad (10)$$

This set of reaction-diffusion equations combined with a moving immersion reagent interface accurately reproduces the patterning produced in experiments. For the Python3 code of this model see the supporting information.

Supporting Information

Supporting Information is available from the Wiley Online Library or from the author.

Acknowledgements

We thank Ricardo Struik for providing the concept drawing used in Figure 1B. We thank the "Advanced Soft Materials" consortium led by Prof. K.U. Loos for fruitful discussions. This research received funding from the Dutch Research Council (NWO) in the framework of the ENW PPP Fund for the top sectors and from the Ministry of Economic Affairs in the framework of the 'PPS-Toeslagregeling'.

References

[1] P. Ball, *The self-made tapestry: pattern formation in nature*, Oxford University Press, Inc., **1999**.

[2] A. Finnemore, P. Cunha, T. Shean, S. Vignolini, S. Guldin, M. Oyen, U. Steiner, *Nature communications* **2012**, *3*, 1 966.

[3] A. McDougal, B. Miller, M. Singh, M. Kolle, *Journal of Optics* **2019**, *21*, 7 073001.

[4] M. Eder, S. Amini, P. Fratzl, *Science* **2018**, *362*, 6414 543.

[5] E. S. Goerlitzer, R. N. Klupp Taylor, N. Vogel, *Advanced Materials* **2018**, *30*, 28 1706654.

[6] K. R. Phillips, G. T. England, S. Sunny, E. Shirman, T. Shirman, N. Vogel, J. Aizenberg, *Chemical Society Reviews* **2016**, *45*, 2 281.

[7] D. Nepal, S. Kang, K. M. Adstedt, K. Kanhaiya, M. R. Bockstaller, L. C. Brinson, M. J. Buehler, P. V. Coveney, K. Dayal, J. A. El-Awady, L. C. Henderson, D. L. Kaplan, S. Keten, N. A. Kotov, G. C. Schatz, S. Vignolini, F. Vollrath, Y. Wang, B. I. Yakobson, V. V. Tsukruk, H. Heinz, *Nature materials* **2023**, *22*, 1 18.

[8] M. M. Lerch, A. Grinthal, J. Aizenberg, *Advanced Materials* **2020**, *32*, 20 1905554.

[9] A.-D. C. Nguindjel, P. J. de Visser, M. Winkens, P. A. Korevaar, *Physical Chemistry Chemical Physics* **2022**, *24*, 39 23980.

[10] M. R. Begley, D. S. Gianola, T. R. Ray, *Science* **2019**, *364*, 6447 eaav4299.

[11] L. Wågberg, J. Erlandsson, *Advanced Materials* **2021**, *33*, 28 2001474.

[12] H. Han, S. Kallakuri, Y. Yao, C. B. Williamson, D. R. Nevers, B. H. Savitzky, R. S. Skye, M. Xu, O. Voznyy, J. Dshemuchadse, L. F. Kourkoutis, S. J. Weinstein, T. Hanrath, R. D. Robinson, *Nature Materials* **2022**, *21*, 5 518.

[13] J. M. De Teresa, *Nanofabrication: Nanolithography techniques and their applications*, IOP Publishing, **2020**.

[14] Y. Wang, I. Fedin, H. Zhang, D. V. Talapin, *Science* **2017**, *357*, 6349 385.

[15] M. Feldman, *Nanolithography: the art of fabricating nanoelectronic and nanophotonic devices and systems*, Woodhead publishing, **2014**.

[16] B. Öktem, I. Pavlov, S. Ilday, H. Kalaycıoğlu, A. Rybak, S. Yavaş, M. Erdoğan, F. Ö. Ilday, *Nature photonics* **2013**, *7*, 11 897.

[17] G. M. Whitesides, B. Grzybowski, *Science* **2002**, *295*, 5564 2418.

[18] P. Vukusic, J. R. Sambles, *Nature* **2003**, *424*, 6950 852.

[19] R. M. Parker, G. Guidetti, C. A. Williams, T. Zhao, A. Narkevicius, S. Vignolini, B. Frka-Petesic, *Advanced Materials* **2018**, *30*, 19 1704477.

[20] C. N. Kaplan, N. Wu, S. Mandre, J. Aizenberg, L. Mahadevan, *Physics of Fluids* **2015**, *27*, 9 092105.

[21] R. D. Piner, J. Zhu, F. Xu, S. Hong, C. A. Mirkin, *science* **1999**, *283*, 5402 661.

[22] B. Hatton, L. Mishchenko, S. Davis, K. H. Sandhage, J. Aizenberg, *Proceedings of the National Academy of Sciences* **2010**, *107*, 23 10354.

[23] J. J. Richardson, J. Cui, M. Bjornmalm, J. A. Braunger, H. Ejima, F. Caruso, *Chemical reviews* **2016**, *116*, 23 14828.

[24] M. A. Boles, M. Engel, D. V. Talapin, *Chemical reviews* **2016**, *116*, 18 11220.

[25] M. Grzelczak, J. Vermant, E. M. Furst, L. M. Liz-Marzán, *ACS nano* **2010**, *4*, 7 3591.

[26] Y. Xia, G. M. Whitesides, *Annual review of materials science* **1998**, *28*, 1 153.

[27] B. A. Grzybowski, *Chemistry in motion: reaction-diffusion systems for micro-and nanotechnology*, John Wiley & Sons, **2009**.

[28] B. A. Grzybowski, K. J. Bishop, C. J. Campbell, M. Fialkowski, S. K. Smoukov, *Soft Matter* **2005**, *1* 114.

[29] M. C. Cross, P. C. Hohenberg, *Reviews of modern physics* **1993**, *65*, 3 851.

[30] R. E. Liesegang, *Naturwissensch Wochenschr* **1896**, *11* 353.

[31] E. Nakouzi, O. Steinbock, *Science Advances* **2016**, *2*, 8 e1601144.

[32] C. J. Campbell, E. Baker, M. Fialkowski, A. Bitner, S. K. Smoukov, B. A. Grzybowski, *J. Appl. Phys.* **2005**, *97* 126102.

[33] Z. Xing, G. Zhang, J. Ye, Z. Zhou, J. Gao, B. Du, K. Yue, Q. Wang, J. Liu, *Advanced Materials* **2023**, *35*, 7 2209392.

[34] H. Qiao, S. Sun, P. Wu, *Advanced Materials* **2023**, 2300593.

[35] M. Itatani, Q. Fang, I. Lagzi, H. Nabika, *Physical Chemistry Chemical Physics* **2022**, *24*, 4 2088.

[36] H. Nabika, M. Itatani, I. Lagzi, *Langmuir* **2019**, *36*, 2 481.

[37] C. T. van Campenhout, D. N. Ten Napel, M. van Hecke, W. L. Noorduin, *Proceedings of the National Academy of Sciences* **2022**, *119*, 39 e2123156119.

[38] R. Tóth, R. M. Walliser, I. Lagzi, F. Boudoire, M. Düggelin, A. Braun, C. E. Housecroft, E. C. Constable, *Soft Matter* **2016**, *12* 8367.

[39] I. Lagzi, D. Ueyama, *Chemical Physics Letters* **2009**, *468*, 4-6 188.

[40] M. Losi, C. Amrhein, W. Frankenberger Jr, *Reviews of environmental contamination and toxicology* **1994**, 91–121.

[41] T. Isemura, *Bulletin of the Chemical Society of Japan* **1939**, *14*, 6 179.

[42] R. M. Walliser, R. Tóth, I. Lagzi, D. Mathys, L. Marot, A. Braun, C. E. Housecroft, E. C. Constable, *RSC advances* **2016**, *6*, 34 28388.

[43] M. Itatani, Q. Fang, K. Unoura, H. Nabika, *The Journal of Physical Chemistry C* **2018**, *122*, 6 3669.

[44] S. Farkas, G. Holló, G. Schuszter, Á. Deák, L. Janovák, V. Hornok, M. Itatani, H. Nabika, D. Horváth, A. Tóth, et al., *The Journal of Physical Chemistry C* **2021**, *125*, 47 26116.

[45] R. Zakhia Douaihy, M. Al-Ghoul, M. Hmadeh, *Small* **2019**, *15*, 28 1901605.

[46] C. Palmer, E. G. Loewen, *Diffraction grating handbook*, Newport Corporation New York, **2005**.

[47] C. J. Kaiser, *The capacitor handbook*, Springer Science & Business Media, **2012**.

[48] E. Unal, A. Gokcen, Y. Kutlu, *IEEE Microwave magazine* **2006**, *7*, 4 48.

Table of Contents

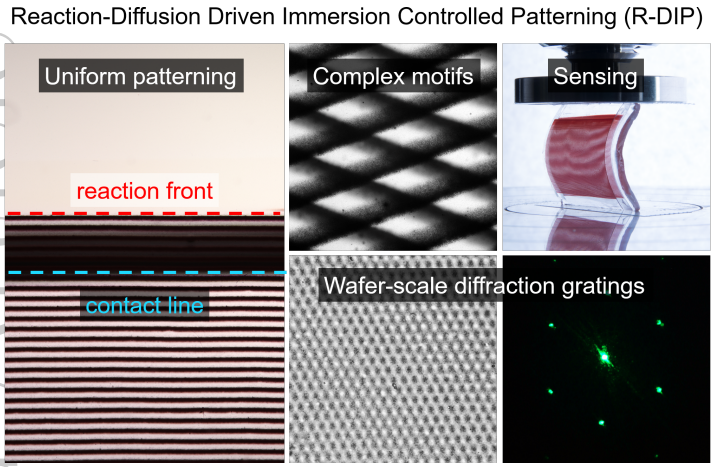

Here we introduce reaction-diffusion driven immersion-controlled patterning (R-DIP). By tying reaction-diffusion processes to immersion we are able to create wafer-scale line motifs. In R-DIP, a balance between diffusion and immersion speed provides robustness towards defects and highly uniform line spacing. We demonstrate the functionality potential of R-DIP by manufacturing tunable optical diffraction gratings and an opto-mechanical sensor.